

B-Spline basis Hartree-Fock method for arbitrary central potentials: atoms, clusters and electron gas

D T Waide, D G Green and G F Gribakin

School of Mathematics and Physics, Queen's University Belfast, University Road,
Belfast BT7 1NN, Northern Ireland, UK

E-mail: dwaide01@qub.ac.uk, d.green@qub.ac.uk, g.gribakin@qub.ac.uk

Abstract. An implementation of the Hartree-Fock (HF) method capable of robust convergence for well-behaved arbitrary central potentials is presented. The Hartree-Fock equations are converted to a generalized eigenvalue problem by employing a B-spline basis in a finite-size box. Convergence of the self-consistency iterations for the occupied electron orbitals is achieved by increasing the magnitude of the electron-electron Coulomb interaction gradually to its true value. For the Coulomb central potential, convergence patterns and energies are presented for a selection of atoms and negative ions, and are benchmarked against existing calculations. The present approach is also tested by calculating the ground states for an electron gas confined by a harmonic potential and also by that of uniformly charged sphere (the jellium model of alkali-metal clusters). For the harmonically confined electron-gas problem, comparisons are made with the Thomas-Fermi method and its accurate asymptotic analytical solution, with close agreement found for the electron energy and density for large electron numbers. We test the accuracy and effective completeness of the excited state manifolds by calculating the static dipole polarizabilities at the HF level and using the Random-Phase Approximation. Using the latter is crucial for the electron-gas and cluster models, where the effect of electron screening is very important. Comparisons are made for with experimental data for sodium clusters of up to ~ 100 atoms.

Keywords: Hartree-Fock, atoms, clusters, electron gas, B-splines

1. Introduction

Much of computational and theoretical atomic physics and chemistry relies on accurate electronic structure calculations. The general N -electron problem is, however, intractable. A favoured starting point for electronic structure calculations of atoms, molecules and nanostructures is the Hartree-Fock (HF) approximation [1–3]. This self-consistent-field approximation treats each electron as if it were moving in the field of the nuclei and the mean field of all the electrons. This can provide a good first approximation and even be sufficient in simple problems. Moreover, the corresponding electronic states can also be used a basis for higher-order calculations that account for post-HF correlations, e.g., using many-body theory (see e.g., [4–8]).

Convergence of methods which aim to achieve self-consistency by iterations is not guaranteed. Recent investigation has shown that convergence of Hartree-Fock-like problems exhibits a fractal nature based on the choice of parameters used [9]. This makes it impossible to predict whether or not the method will converge for a given system. Special measures need to be taken to ensure that iterations for a large class of systems converge and that they converge quickly. Here, we use a numerical implementation of the self-consistent Hartree-Fock equations based on a B-spline approach and a new algorithm for achieving self-consistency (BSHF) [10] that allows the use of arbitrary central potentials. Specifically, convergence is aided by gradually increasing the magnitude of the electron-electron Coulomb interaction to its true value. We show that it provides good convergence properties for difficult systems such as negative ions, or electrons confined by a weak harmonic potential [11] (for which traditional convergence methods failed, and for which we compare with the results of the Thomas-Fermi method). We calculate static dipole polarizabilities at the HF level and using the Random-Phase Approximation (RPA) to assess the degree of completeness of the excited state manifold. This understanding is important for future applications, such as studying the interaction of a positron and electrons in a harmonically confined electron gas [12] using many-body theory methods [13, 14].

2. Hartree-Fock method and its present B-spline basis numerical implementation

The relevant HF equations and the numerical implementation used here are described fully in Ref. [10]. In the Hartree-Fock approximation [1–3], the total wavefunction of an N -electron system of energy E is approximated by a Slater determinant (or sum of Slater determinants, in general) that is an antisymmetrised product of N single-electron spin orbitals $\phi_{\alpha_j}(x_j)$, viz. $\Psi_E(x_1, \dots, x_N) = \sqrt{N!} \hat{\mathcal{A}} \prod_{j=1}^N \phi_{\alpha_j}(x_j)$, where $\hat{\mathcal{A}}$ is the antisymmetrisation operator, α_j represents a complete set of quantum numbers describing the j -th orbital, and $x_j = (\mathbf{r}_j, \sigma_j)$ represents the electron position and spin. Minimising the expectation value of the Hamiltonian through the variation of the ϕ_{α} , or, in the diagrammatic approach, summing a certain class of diagrams [15, 16], yields the system of N integro-differential equations, the Hartree-Fock equations, for the electron orbitals $\phi_{\alpha_j} \equiv \phi_j$ and single-particle energies ε_j , in atomic units,

$$\left(-\frac{1}{2} \nabla^2 + V(r) + \hat{V}^{\text{HF}} \right) \phi_j(x) = \varepsilon_j \phi_j(x). \quad (1)$$

Here the first term in the bracket is the kinetic energy operator, and the second term is a local central potential $V(r)$. For an atom with atomic number Z , $V(r) = -Z/r$, but in the BSHF program [10] it can also be chosen to be an arbitrary central potential, e.g., a harmonic confining potential, for a system of electrons to approximate the electron gas in the background of a uniform positive-charge distribution [17]. The Hartree-Fock potential $\hat{V}^{\text{HF}} = \sum_{i=1}^N \left(\hat{J}_i - \hat{K}_i \right)$ is a sum of the direct and (non-local) exchange terms

$\hat{J}_i\phi_j(x) = \int dx_i \phi_i^*(x')\rho^{-1}\phi_i(x')\phi_j(x)$ and $\hat{K}_i\phi_j(x) = \int dx_i \phi_i^*(x')\rho^{-1}\phi_j(x')\phi_i(x)$, where $\rho = |\mathbf{r}' - \mathbf{r}|$. Equation (1) demands a self-consistent solution due to the interdependency of the Coulomb mean field potential \hat{V}^{HF} and the electron orbitals ϕ_j . Beyond this, the resulting ground-state orbitals can be held *frozen*, i.e. constant, while an additional electron or positron is introduced and the wavefunction of this extra particle in the presence of the *frozen core* is subsequently found, enabling generation of excited-state bases for higher-order many-body calculations.

For a spherical system confined by a central potential $V(r)$, single-particle wavefunctions can be written in terms of their radial, angular and spin components,

$$\phi_{nlm\sigma}(x) = r^{-1}P_{nl}(r)Y_{lm}(\theta, \phi)\chi_{\sigma}, \quad (2)$$

where P_{nl} is the radial wavefunction, Y_{lm} is the spherical harmonic and χ_{σ} is the spin part.

In the case of a closed-shell system, each spatial electronic orbital is occupied by two electrons with antiparallel spins. For a closed-shell atom or another spherical system, the solution of the HF equations reduces to a *central-field problem*, i.e. the potential is spherically symmetric, leading to the radial Hartree-Fock equations,

$$-\frac{1}{2}\frac{d^2}{dr^2}P_i(r) + \left[V(r) + \frac{l(l+1)}{2r^2} + V_{\text{dir}}(r) \right] P_i(r) + \int_0^{\infty} U(r, r')P_i(r')dr' = E_iP_i(r), \quad (3)$$

where i is a composite label for the orbitals of quantum numbers nl . Here $V_{\text{dir}}(r)$ is the local direct (Hartree) potential, representing the interaction between a single particle and the average field of the other particles, and $U(r, r')$ is the non-local exchange kernel (the ‘‘Fock term’’), which is the interaction between two particles due to the exchange of their coordinates (see [10] for detailed expressions).

Equation (3) may also be used for open-shell electronic configurations under the further approximation of spherical averaging of the wavefunctions. In the case of the ground state for open-shell neutral atoms this difference is relatively small since the variation from the ideal case arises due to only one incomplete subshell.

Wavefunctions of excited electron states can also be obtained from Eq. (3). Physically, they describe an electron added to the ground-state of N electrons. In the case of an additional electron in a system with s ground-state orbitals, the wavefunction of the additional particle, $i > s$, is found from Eq. (3) with $V_{\text{dir}}(r)$ and $U(r, r')$ fixed by the self-consistent ground-state calculation of the first s orbitals. For positrons, one simply drops the exchange term and makes appropriate changes of sign to account for its opposite charge.

2.1. Hartree-Fock equation in the B-spline basis

B-splines $B_{i,k}$ of order k are piecewise polynomials of degree $k - 1$ defined over a restricted domain (‘‘box’’) that is divided into $n - k + 1$ segments by a knot sequence of n points: $r_i \in [0, R]$, where $i = 1, \dots, n$ and n is the number of non-zero splines in the basis [18]. We use an exponential knot sequence to ensure that the wavefunctions are

represented accurately near the nucleus where they vary more rapidly, and to minimise computational expense in regions far from the nucleus where the wavefunction varies least rapidly. Such knot sequences also generate sets of excited states that ensure rapid convergence of perturbation-theory sums and are useful in many-body theory calculations [13]. By varying the parameters of the sequence, one can make it almost equidistant, which is useful for studying a harmonically confined electron gas and models of clusters.

The radial wavefunction is expanded in terms of B-splines, $P_i(r) = \sum_j c_j^{(i)} B_j(r)$, where we have dropped the second subscript in the B-splines. Projecting the radial Hartree-Fock equation for a given angular momentum l onto an arbitrary basis function $B_k(r)$ gives the generalized eigenvalue problem, $\mathcal{H}^{(l)} \mathbf{c}^{(l)} = E \mathcal{B} \mathbf{c}^{(l)}$, where

$$\mathcal{H}_{ij}^{(l)} = \int_0^R \left\{ \frac{1}{2} \frac{dB_i}{dr} \frac{dB_j}{dr} + B_i(r) \left[V(r) + \frac{l(l+1)}{2r^2} + \hat{V}_{\text{HF}} \right] B_j(r) \right\} dr, \quad (4)$$

$\mathcal{B}_{ij} = \langle B_i | B_j \rangle$ is the B-spline overlap matrix, $\mathbf{c}^{(l)}$ is the vector of coefficients for angular momentum l , $V(r)$ is the local central potential, and \hat{V}_{HF} is the Hartree-Fock potential. Note that to implement the boundary conditions $P(0) = P(R) = 0$, the first and last splines are discarded in the expansions. The eigenvalue problem is computationally easier to solve than the original set of integro-differential equations. The integrals are calculated using Gauss-Legendre quadrature, splitting the integration interval into two sections in the elements where a cusp is present [10].

2.2. Convergence of iterations

In our approach, the electron potential is calculated, starting with the wavefunctions in the potential $V(r)$ (i.e., $\hat{V}_{\text{HF}} = 0$), and the eigenvalue problem is solved repeatedly until the difference in successive approximations of the wavefunction and energy decreases below a certain tolerance ε , i.e., when $\eta_i < \varepsilon$ for all orbitals, where η_i is defined as

$$\eta_i = \max \left(\left| P_i^{(m)}(r) - P_i^{(m+1)}(r) \right|, \left| E_i^{(m)} - E_i^{(m+1)} \right| \right). \quad (5)$$

The HF problem is initially solved only for values of orbital angular momentum represented by the occupied orbitals. Once the solutions of the occupied orbitals are self-consistent to tolerance ε , the excited electron or positron states are calculated for all required values of the angular momentum.

To ensure that the solutions converge towards the true ground state of the many-electron system and do not get ‘stuck’ on local minima representing excited states or fail to converge, being caught in a cycle of distinct solutions, it is necessary to employ a number of strategies. In particular, the strength of the elementary charge e is initially chosen to be smaller than unity so that the effect of the electron-electron interaction on the solution to the HF equations is suppressed. The HF problem is solved using this reduced interaction. Once self-consistent solutions have been determined, the strength of the elementary charge used in the electron-electron interaction, e_m , is increased towards

unity according to

$$e_m = 1 - \frac{1}{2}e_s^m, \quad m = 1, \dots, m_{\max}, \quad (6)$$

where typically $e_s \sim 0.15$ – 0.5 , and m_{\max} is the number of increments to take before setting the charge to unity, and iterating further until self-consistency is reached.

To improve the rate at which the solution converges, in particular, when iterations are trapped in a cycle, the new wavefunctions may be calculated as a linear combination of the current iteration and the previous one, viz.,

$$P_{i,est}^{(m)}(r) = (1 - \alpha)P_i^{(m)}(r) + \alpha P_i^{(m-1)}(r), \quad (7)$$

where the coefficient α is calculated as

$$\alpha = \frac{E_i^{(m)} - E_i^{(m-1)}}{E_i^{(m)} - 2E_i^{(m-1)} + E_i^{(m-2)}}, \quad (8)$$

a scheme utilised by Amusia and Chernysheva in the *hfgr* code [19].

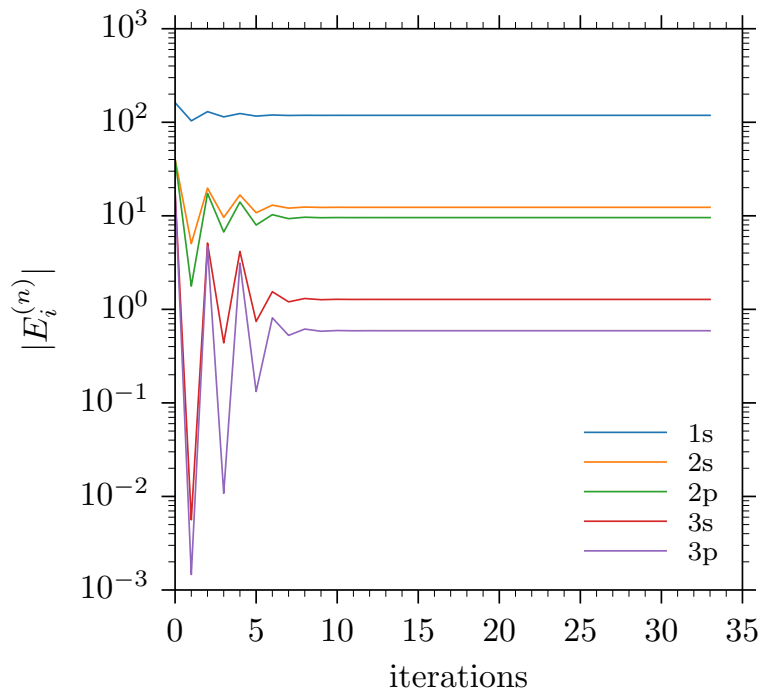


Figure 1. Convergence of the occupied electron orbital energies for Ar against the number of iterations of the self-consistency process using $n = 40$ splines of order $k = 6$. No special techniques were necessary for the iterations to converge.

Most closed shell neutral atoms converge without any special treatment. Figure 1 shows the progression of energies of occupied orbitals with iterations of the self-consistency process for Ar. Negative ions are more unstable. Figure 2 shows the analogous plot for the isoelectronic negative ion Cl^- . The grey lines show that without additional measures, the system oscillates between two states and the iterations do not converge. The coloured lines are also for Cl^- , but with the elementary charge gradually

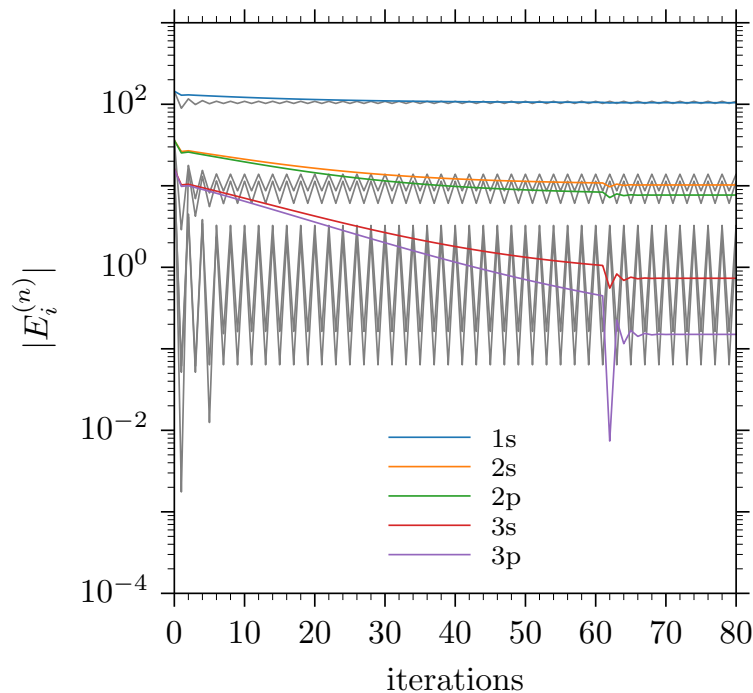


Figure 2. Convergence of the occupied orbital energies for a negative ion, Cl^- , with no ‘annealing’ of the electron-electron interaction (grey), and the same system converged using annealing with parameters $e_s = 0.15$, $m_{\text{max}} = 50$ (colours).

increased from 0.15 to 1.0. This is sufficient for achieving convergence for this system to the required $\varepsilon = 10^{-12}$ threshold.

One exception to the easy convergence displayed by for neutral atoms is Zn. Figure 3 shows that even using the electron-electron interaction ‘annealing’, the solution becomes unstable beyond a certain point ($e_m \approx 1 - 10^{-5}$). This attempt is represented by the grey lines. The coloured lines are for the same system but using a linear combination of the current and previous estimate of the self-consistent solution, Eq. (7), which allows the iterations for Zn to converge.

The combination of these two techniques with sensible values of e_s and m_{max} allows rapid calculation of the ground- and excited- state energies and wavefunctions for a wide variety of systems, including neutral atoms and negative ions, as well as the electron gas confined by less singular, e.g., harmonic, potentials.

3. Results for neutral atoms

To demonstrate the robustness of the approach, we first consider neutral noble gas atoms. The computed ground-state energies of each orbital and the total energy are shown in Table 1 with comparison to reference Hartree-Fock data by Saito [20] and also experimental data [21, 22]. The calculations were performed using $n = 40$ B-splines (in fact 38, as the first and the last B-spline are dropped, to satisfy the boundary conditions) of order $k = 6$ to a self-consistent absolute error of 10^{-12} . The tabulated values show

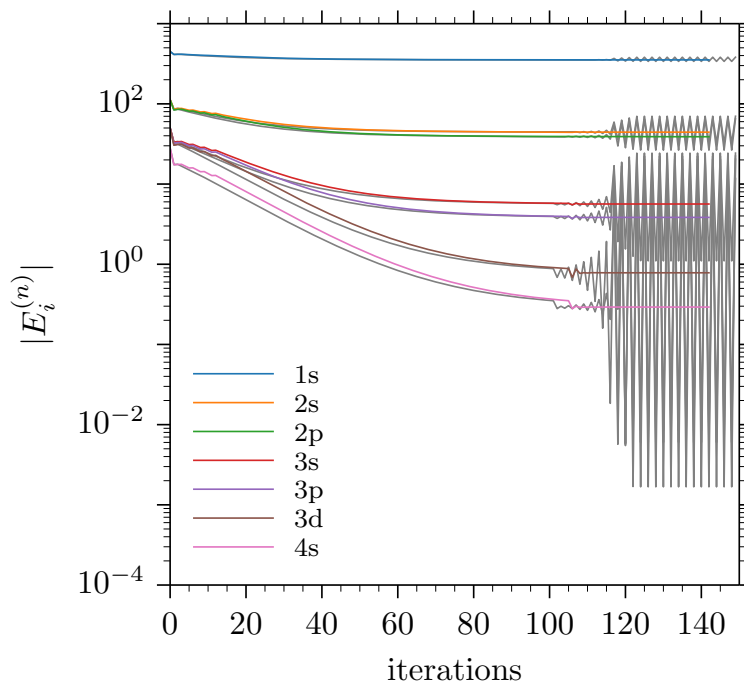


Figure 3. Convergence of the electron orbital energies of Zn using ‘annealing’ of the electron-electron interaction, Eq. (6) with $e_s = 0.9$, grey lines, and using ‘mixing’ of the current and previous estimates of the solution, Eq. (7) (coloured lines).

that the calculated orbital energies are accurate to $\sim 10^{-6}$ a.u. with respect to the reference data.

Heavier atoms stretch the limits of the nonrelativistic HF approximation and improving the code to use the Dirac-Fock formalism should increase the performance in this regime. It can also be seen that, with the exception of the heaviest atom, radon, the results are within a few percent of the experimental ionization energy values.

Example sets of wavefunctions are shown in Figure 4 for Ne and Kr. Note that in both graphs the asymptotic behaviour of all the orbitals is similar to that of the outermost orbital, as expected from Handy *et al.* [23], who found that the asymptotic behaviour of Hartree-Fock orbitals is proportional to the exponential of the orbital i with the highest energy, i.e., the valence orbital,

$$P_j(r) \propto \exp\left(-\sqrt{2|E_i|r}\right). \quad (9)$$

This is a consequence of the nonlocal exchange interaction between the electrons, as for a local potential the asymptotic behaviour would be $P_j(r) \propto \exp\left(-\sqrt{2|E_j|r}\right)$. Dzuba *et al.* [24] also noticed that the exchange interaction leads to additional nodes in some of the wavefunctions, increasing them above the expected $n-l-1$ (i.e., the radial quantum number); see [25] for further background, additional references and physical implications. In Ne, shown in Fig. 4 (a), the 1s wavefunction has zero nodes, as expected. In Kr, Fig. 4 (b), however, it has two nodes which show as downward cusps on the logarithmic scale. These extra nodes were considered “undesirable” in the past. However, arguments

Table 1. Absolute values of the electron orbital energies and total ground-state energies for noble gas atoms calculated in the present work vs. reference Hartree-Fock calculations [20] and experimental data [21, 22].

nl	Energies (a.u.) for He, $Z = 2$			Energies (a.u.) for Ne, $Z = 10$		
	Present	Ref. [20]	Exp.	Present	Ref. [20]	Exp.
1s	0.917955570	0.917956	0.904	32.772442840	32.772443	31.982
2s				1.930390950	1.930391	1.781
2p				0.850409731	0.850410	0.792 ^b
E_{tot}	2.861679994	2.861679996		128.547098291	128.547098109	
nl	Energies (a.u.) for Ar, $Z = 18$			Energies (a.u.) for Kr, $Z = 36$		
	Present	Ref. [20]	Exp.	Present	Ref. [20]	Exp.
1s	118.610350525	118.610351	117.818	520.165468002	520.165468	526.508
2s	12.322153702	12.322153	11.991	69.903082341	69.903082	70.669
2p	9.571466070	9.571466	9.160	63.009785490	63.009785	62.315
3s	1.277354057	1.277353	1.075	10.849466647	10.849466	10.768
3p	0.591018393	0.591017	0.579	8.331501615	8.331501	7.977
3d				3.825234561	3.825234	3.465
4s				1.152935491	1.152935	1.011
4p				0.524187023	0.524187	0.514
E_{tot}	526.817519726	526.817512803		2752.054982444	2752.054977350	
nl	Energies (a.u.) for Xe, $Z = 54$			Energies (a.u.) for Rn, $Z = 86$		
	Present	Ref. [20]	Exp.	Present	Ref. [20]	Exp.
1s	1224.397777074	1224.397777	1270.093	3230.312837069	3230.312828	3616.134
2s	189.340123037	189.340123	200.394	556.913115482	556.913115	663.436
2p	177.782448960	177.782449	179.839	536.676971452	536.676971	570.411
3s	40.175663257	40.175663	42.225	138.421866638	138.421866	164.637
3p	35.221661899	35.221662	35.328	128.671558522	128.671558	137.504
3d	26.118869411	26.118869	25.056	110.701350357	110.701350	108.043
4s	7.856302172	7.856302	7.839	33.920746766	33.920746	40.241
4p	6.008338645	6.008338	5.488	29.491183982	29.491183	31.114
4d	2.777881328	2.777881	2.510	21.331318412	21.331318	20.102
4f				10.107636171	10.107635	8.531
5s	0.944414880	0.944414	0.860	6.905819457	6.905818	7.901
5p	0.457290527	0.457290	0.446	5.225212748	5.225212	5.182
5d				2.326320041	2.326319	1.838
6s				0.873993818	0.873993	0.884 ^a
6p				0.428007511	0.428007	0.430 ^a
E_{tot}	7232.138377815	7232.138363870		21866.772281217	21866.7722409	

^aEnergies from the NIST Atomic Spectra Database [22].

^bFor orbitals with $l \geq 1$, the experimental energies are statistical averages of the fine-structure components, except for the outer np orbital, where the value of the ionization potential is shown.

have been made recently that they may be responsible for observable effects such as the shapes of gamma-ray-spectrum peaks in positron-atom annihilation, the width of which is affected by annihilation on the inner shell electrons enhanced by exchange-assisted tunnelling [25].

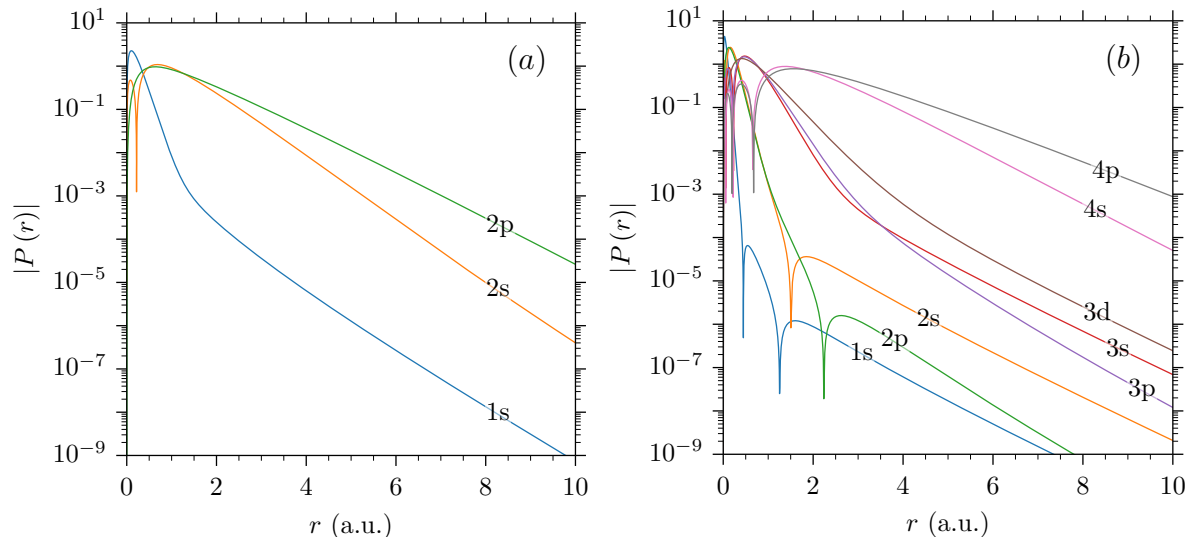


Figure 4. The set of ground-state wavefunctions of (a) Ne, and (b) Kr, calculated using 100 B-splines of order 9, with $R = 30$ a.u. In (a) the wavefunctions have $n - l - 1$ nodes, which appear as cusps when plotted on a log scale. However, in Kr (b) the inner orbitals exhibit extra nodes due to the exchange interaction [24].

4. Results for harmonically confined electron gas: comparison between Hartree-Fock and the Thomas-Fermi model

We now investigate the confinement of N electrons in a harmonic potential

$$V(r) = \frac{1}{2}\omega^2 r^2, \quad (10)$$

which is equivalent to a background field of constant positive charge density $\rho_b = \nabla^2 V / 4\pi = 3\omega^2 / 4\pi$. This can be viewed as the simplest model for a metallic cluster, with N free electrons in the background potential of N singly-ionised (e.g., alkali) atoms distributed evenly in space (the “jellium” model).

We have calculated the orbital wavefunctions and energies for harmonic potentials with $\omega = 1$ and $\omega = 0.1$ a.u., for a series of closed-shell N -electron systems with $N \leq 58$. In what follows we compare the results obtained using the Hartree-Fock approximation with those of the simpler Thomas-Fermi method, expected to be applicable for $N \gg 1$.

4.1. Hartree-Fock calculations for harmonically confined electron gas

The Hartree-Fock calculations were performed using the BSHF code [10] with $n = 40$ B-splines of order $k = 6$. The ground-state orbital and total energies are shown in Tables

2 and 3, in which successive columns show the energies for a system with an extra fully occupied orbital added, starting from the $1s^2$ configuration in the left-most column. Note that for consistency we continue to use the hydrogenic orbital notation. Figure 5

Table 2. Energies of electron orbitals nl and the total energy E_{tot} for closed-shell systems with up to 40 electrons in a harmonic potential with $\omega = 1$. Also shown is the number of iterations required to converge to an accuracy of 10^{-12} .

N	2	8	18	20	34	40
nl	$1s^2$	$+2p^6$	$+3d^{10}$	$+2s^2$	$+4f^{14}$	$+3p^6$
# iter.	112	116	127	127	175	177
E_{tot}	3.771808	32.924181	121.395738	143.656801	340.876811	444.108657
1s	2.259377	5.213001	9.168740	9.910487	14.372843	16.212245
2p		6.015730	9.747907	10.464158	14.842209	16.599356
3d			10.467192	11.143587	15.370154	17.084543
2s				11.291091	15.520892	17.241711
4f					16.007277	17.672330
3p						17.886544

Table 3. Energies of electron orbitals nl and the total energy E_{tot} for closed-shell systems with up to 40 electrons in a harmonic potential with $\omega = 0.1$. Also shown is the number of iterations required to converge to an accuracy of 10^{-12} .

N	2	8	18	20	34	40
nl	$1s^2$	$+2p^6$	$+3d^{10}$	$+2s^2$	$+4f^{14}$	$+3p^6$
# iter.	120	126	139	139	147	154
E_{tot}	0.529043	5.862360	23.198236	27.725662	67.695891	89.033498
1s	0.369424	1.097304	2.003531	2.164581	3.161704	3.552365
2p		1.170797	2.044064	2.205478	3.193091	3.577094
3d			2.113414	2.268952	3.233674	3.616198
2s				2.292318	3.252050	3.641505
4f					3.294960	3.672200
3p						3.702001

shows the energies of the occupied and excited-state orbitals for a system with $N = 58$ electrons for $\omega = 1$ and $\omega = 0.1$ a.u. The excited-state orbitals describe the states of an electron added to the system. The stronger confining harmonic potential with $\omega = 1$ a.u. makes the energy-level spectrum closer to that of the harmonic oscillator.

Figure 6 shows the charge density of closed-shell systems with $N = 2, 8, 18, 20, 34, 40$ and 58 electrons. It can be seen that the radius of the system increases as more electrons are added and as the angular frequency (ω) is reduced from 1 a.u. to 0.1 a.u. As electrons are added, the density becomes more uniform and closer to the positive background charge density ρ_b shown by the grey dotted line. Indeed, as N becomes large, the electron density acts to cancel out the positive background density giving the

asymptotic relationship between N , ω , and system radius R as for a classical uniformly charged sphere, with $N \approx 4\pi R^3/3\rho_b$, i.e., $R \approx N^{1/3}/\omega^{2/3}$.

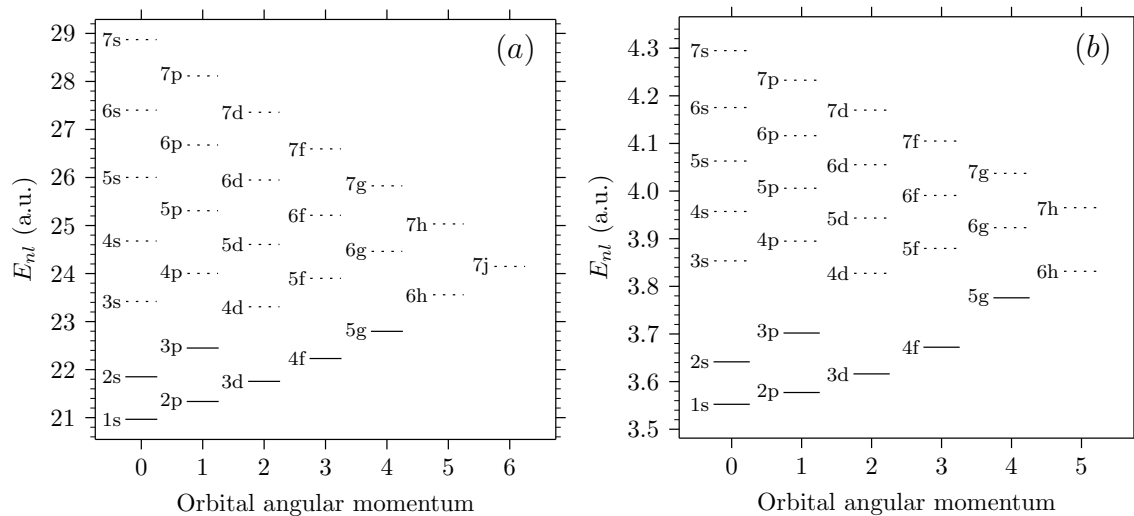


Figure 5. The ground and excited-state electron energy levels for a system of 58 electrons in a harmonic potential, (a) $\omega = 1.0$ a.u., and (b) $\omega = 0.1$ a.u.; solid lines indicate occupied orbitals, dotted lines — excited states.

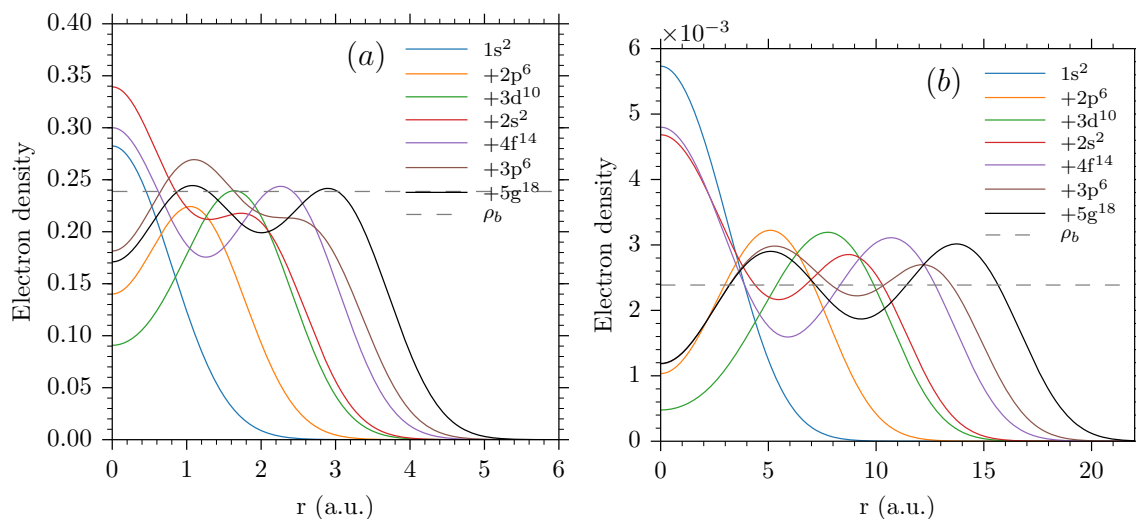


Figure 6. The electron density for a harmonic well with an increasing number of electrons in closed shells for (a) $\omega = 1.0$ a.u., and (b) $\omega = 0.1$ a.u. Each successive line represents the density of the next closed-shell system, up to a total of 58 electrons.

4.2. Thomas-Fermi approximation

To further test the validity of the results for the harmonically confined electron gas, we also analysed this system by adapting the well-known Thomas-Fermi method [26], a semi-classical approximation for a system of electrons in which its state is represented

by the electron density rather than a set of single-particle wavefunctions. It is often thought of as a precursor to the modern-day density functional theory, and although it fails to predict features of realistic systems, such as electronic shell structure, it is still often used since a qualitative view of the asymptotic behaviour of a system can be found comparatively easily [27, 28]. This semi-classical approximation treats the electrons as occupying a density of states in phase space,

$$dN_e = 2 \cdot \frac{4\pi p^3}{3(2\pi)^3} dV, \quad (11)$$

where a factor of 2 has been included for spin degeneracy. Assuming that each of the electrons has a maximum single-particle energy given by,

$$\varepsilon_0 = \frac{1}{2}p_0^2 + \frac{1}{2}\omega^2 r^2 - \phi_e, \quad (12)$$

where p_0 is the maximum electron momentum, the distribution of the electrons can be found from Poisson's equation,

$$\nabla^2(\phi_{bg} + \phi_e) = 4\pi(n_e - \rho_{bg}), \quad n_e = -\rho_e, \quad (13)$$

where ϕ_{bg} and ϕ_e are the harmonic background potential and the potential due to the charge distribution, n_e . The harmonic potential is equivalent to a constant background charge density, $\rho_{bg} = 3\omega^2/4\pi$. Note that, in atomic units, the electronic charge distribution and equivalent potential differ by a factor of -1 .

Expanding the Laplacian in Poisson's equation, and assuming that the electron and background potentials are spherically symmetric, gives the non-linear differential equation,

$$\frac{d^2 n_e}{dr^2} = \frac{1}{3}n_e^{-1} \left(\frac{dn_e}{dr} \right)^2 - 2r^{-1} \frac{dn_e}{dr} + \frac{4\pi}{B} n_e^{4/3} - \frac{3\omega^2}{B} n_e^{1/3}, \quad (14)$$

where $B = (\pi^4/3)^{1/3}$.

We take the electrons to be confined by the harmonic potential within a spherical box of radius R_e such that the electron charge density falls to zero everywhere outside this box. Given that the harmonic potential tends to zero at the centre of the box, charge density of the electrons will approach a constant value, n_0 , close to the centre, and at $r = 0$ we assume that it is constant. These considerations constrain solutions of the ODE to satisfy the boundary conditions,

$$n_e(0) = n_0, \quad \left. \frac{dn_e}{dr} \right|_{r=0} = 0, \quad n_e(r) = 0, \quad r \geq R_e. \quad (15)$$

Integrating the charge density across the volume of the box must then give the total number of electrons in the system,

$$4\pi \int_0^{R_e} r^2 n_e dr = N_e. \quad (16)$$

It can be readily seen from equation (14) by substitution of the boundary conditions that for n_e to decrease to zero then the initial charge density must satisfy $n_0 < 3\omega^2/4\pi = n_{bg}$.

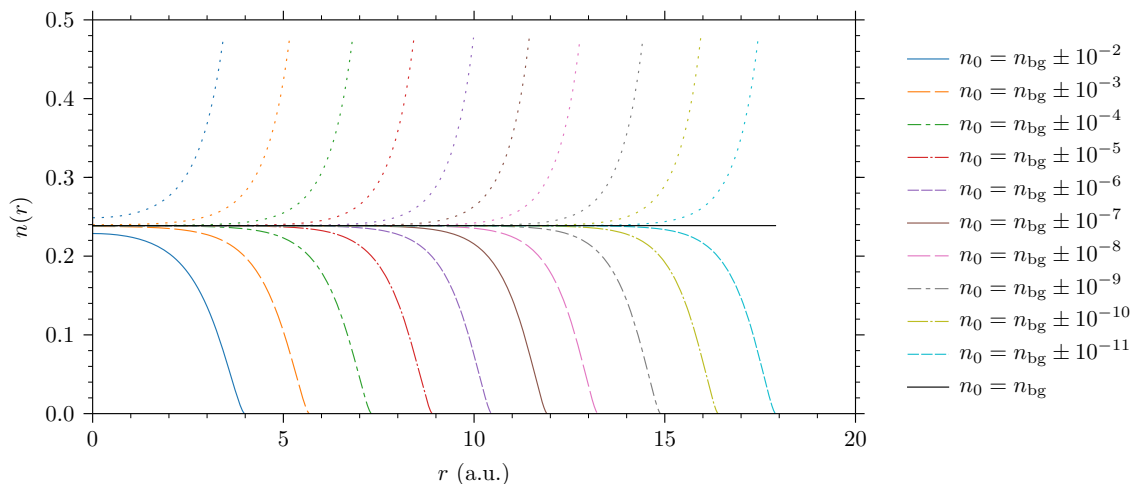


Figure 7. Limits to the solution of the 1-D harmonic Thomas-Fermi equation ($\omega = 1.0$). The black line is the background charge density n_{bg} , also the boundary between physical and unphysical solutions. Solutions with initial charge density $n_0 \geq n_{\text{bg}}$ diverge, whereas solution with $n_0 < n_{\text{bg}}$ reduce to 0 at some point $r = R_e$.

Solutions to equation (14), constrained by the conditions (15) and (16) are shown in Figure (7) for a range of values of the parameterised boundary condition, the initial charge density, n_0 . The boundary between physical and unphysical solutions, where $n_0 = n_{\text{bg}}$ is shown as a solid black line. Solutions with $n_0 > n_{\text{bg}}$, shown as dotted lines, are monotonically increasing and therefore cannot represent systems with a finite number of electrons. The physical solutions show that the size of the system R_e increases approximately linearly with an order of magnitude decrease in the difference between n_0 and n_{bg} . When solving the ODE numerically care must be taken to ensure that sufficient numerical precision is used. As ω decreases the required precision increases, e.g. for $\omega = 0.1$, 40 significant figures are required to distinguish between systems with varying numbers of electrons.

To allow comparison with the Hartree-Fock results we need to be able to relate n_0 with the number of electrons in the system, N . We solve the ODE for a range of n_0 values and calculate the corresponding N by integration, as per equation (16). A non-linear function, described in section 4.2.2, is then fitted to these points and used to compute n_0 for any desired N .

4.2.1. Non-interacting solution. Equation (14) is non-linear, and therefore likely intractable analytically. However, a simple analytical solution may be found by ignoring the term arising from interaction between pairs of electrons, simplifying the equation. This gives the electron number density as,

$$n(r) = \frac{1}{3\pi^2} (2\varepsilon_0 - \omega^2 r^2)^{3/2}. \quad (17)$$

However, this is an over-simplification as the results deviate significantly from those of the full numerical solution. Comparing the magnitude of the energy of the interaction

between pairs of electrons, $E_{\text{pot}}^{(2)}$, with that of the harmonic potential energy, V , we can see that this approximation is only valid when $N \ll w$, i.e. as the electrons are more tightly bound their interaction with each other becomes less important. We do not consider this approximation further.

4.2.2. Asymptotic solution. Another way to arrive at an analytical expression for $n(r)$ is to consider its asymptotic form as N_e becomes large. Introducing the dimensionless function $\tilde{\eta}(r)$ defined by

$$n(r) = n_{\text{bg}} \left(1 - \frac{\tilde{\eta}(r)}{r} \right), \quad (18)$$

and taking the ansatz

$$\tilde{\eta}(r) = A_1 \exp(\beta r) + A_2 \exp(\gamma r), \quad A_1, A_2, \beta, \gamma \in \mathbb{R}, \quad (19)$$

in Eqn. (14) results in the solution

$$\tilde{\eta}(r) = \frac{\eta_0}{\beta} \sinh(\beta r), \quad \eta_0 = 1 - \frac{n_0}{n_{\text{bg}}}. \quad (20)$$

From this, the asymptotic form for the radius is found to be

$$R_e \simeq P + Q \ln(n_{\text{bg}} - n_0). \quad (21)$$

Given that the electrons are trapped in a spherical box, it may be assumed that the mutual repulsion of the electrons leads to them being evenly distributed as their number becomes large. This makes the system similar to that of the uniformly charged insulating sphere. Therefore we take the relationship between the radius and the number of electrons to have the same form, $R_e \sim N_e^{1/3}$.

4.2.3. Energies. For comparison with Hartree-Fock the total energy of the system, along with the kinetic, 1-body potential, and 2-body potential energies were calculated as follows.

$$E_t = E_{\text{kin}} + E_{\text{pot}}^{(1)} + E_{\text{pot}}^{(2)}, \quad (22)$$

$$E_{\text{kin}} = 4\pi\chi \int_0^\infty n^{5/3} r^2 dr, \quad \chi = \frac{3}{10} (3\pi^2)^{2/3}, \quad (23)$$

$$E_{\text{pot}}^{(1)} = 2\pi\omega^2 \int_0^\infty nr^4 dr, \quad (24)$$

$$E_{\text{pot}}^{(2)} = \frac{1}{2} \iint d^3\mathbf{r} d^3\mathbf{r}' \frac{n(r)n(r')}{|\mathbf{r} - \mathbf{r}'|}. \quad (25)$$

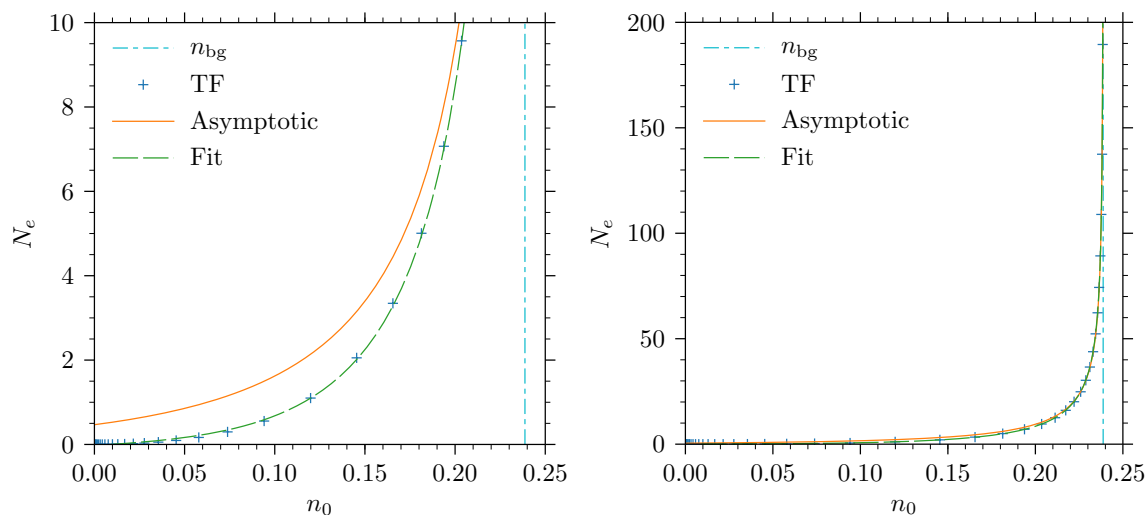


Figure 8. The number of electrons in the system, N_e against the parametrized boundary condition, n_0 for a harmonic potential with $\omega = 1$ in the Thomas-Fermi approximation with positive background charge density n_{bg} (vertical line). “TF” is the Thomas-Fermi result (plus symbols), i.e., the discrete solutions of Eqns. (14–16). “Asymptotic” is the fit using expression Eqn. (21) taking $R_e \sim N_e^{1/3}$ (orange line), and “fit” that using Eqn. (26) (green-dashed line).

4.2.4. Fitting model. Electron number density curves $n(r)$ were computed for a range of values of n_0 , distributed such that the values became more closely spaced as n_0 approached n_{bg} . The number of electrons represented by each solution was then calculated by integrating over $n(r)$.

Figure (8) shows N_e plotted against the parameter n_0 for system with $\omega = 1$. The dot-dashed line is the density corresponding to the positive background charge density n_{bg} . The data has been fitted to the asymptotic behaviour function in Eqn. (21). The same data has been shown at two different ranges for N_e , and it is clear from the figure that the function does fit the relationship for large values of N_e (right panel) but not for smaller values (left panel). Indeed, in the limit as n_0 tends to zero, the number of electrons does not become zero. The relationship is almost quadratic for small N_e so additional terms were added to the model to improve the fit for small N_e , giving

$$N_e \simeq [P + Q \ln(n_{\text{bg}} - n_0)]^3 + C_1 n_0^2 + C_2 n_0 + C_3, \quad C_i \in \mathbb{R}, \quad (26)$$

shown in Fig. (8) as the dashed line, the pragmatic fit. This now provides a good method of choosing the parameter n_0 corresponding to a system with a given number of electrons, N_e . This can be validated by integration once the solution, $n(r)$, is found.

4.3. Comparison between Thomas-Fermi and Hartree-Fock

In Fig. (9) the electron number densities, $n_e(r)$, have been shown for systems with ω (in the range 0.1–1) and N_e (in the range 2–106). The radius of the system — determined

Table 4. The kinetic, one-body and two-body potential components of the total energy for systems with various ω and N_e , comparing the results of HF calculations with those of the Thomas-Fermi method.

ω	N_e	E_{kin}		$E_{\text{pot}}^{(1)}$		$E_{\text{pot}}^{(2)}$	
		HF	TF	HF	TF	HF	TF
0.1	2	0.1071	0.0730	0.2121	0.2569	0.2098	0.3678
0.1	20	1.0299	0.8939	9.5853	10.2809	17.1105	18.7742
0.1	106	5.5175	5.0238	153.7706	157.474	296.5061	304.903
1.0	2	1.3187	1.0819	1.7090	1.8124	0.7536	1.4611
1.0	20	17.0992	15.7096	53.6006	55.2399	72.9687	79.0605
1.0	106	101.8276	97.4406	767.4847	780.4820	1331.2867	1366.08

by the point where n_e falls to $10^{-3} \cdot n_e(0)$ — is dependent on ω and N_e ,

$$R_e \propto \sqrt{\omega}, \quad R_e \propto N_e^{1/3}, \quad (27)$$

from comparison with the uniformly charged insulating sphere, and the behaviour of the system at the classical turning point. The plots give a visual comparison of HF calculated density with the results of the simpler Thomas-Fermi model. The analytic solution to TF, in which the electron-electron interaction has been ignored gives a fair approximation of the radius for $N_e = 2$ but not for greater N_e , neither does it predict the form of the radial density curve. It has been ignored for larger systems. The asymptotic solution in Eqn. (20) becomes close to the form of the full numerical solution as N_e becomes large. Both predict the radius well and approximate the form of the HF solution at large N_e . As n_e becomes uniform near the centre, the HF solution oscillates about the TF solution. As the asymptotic and numerical solutions both become similar to HF for large N_e , we can be confident that the HF solutions are credible in this domain, i.e. that of finite numbers of fermions in a centrally-symmetric harmonic potential. Further evidence supporting the similarity of the solutions is given in Table 4 which compares the kinetic, one-body, and two-body components of the total energy of different systems as calculated in both models. For all systems the energies of both models are broadly similar, increasingly so for large N_e where they agree to within a few percent.

5. Polarizability of atoms and atomic clusters

5.1. Atoms

A further test of the suitability of the wavefunctions was made by calculating the static dipole polarizability of the noble gas atoms

$$\alpha = \frac{2}{3} \sum_{nl, n'l'} l_{>} \frac{|\langle n'l' | r | nl \rangle|^2}{E_{n'l'} - E_{nl}}, \quad (28)$$

where $l_{>} = \max\{l, l'\}$ and the sum nl is over occupied orbital and $n'l'$ over excited orbitals. The results are given in Table 5 and are found to be in good agreement with

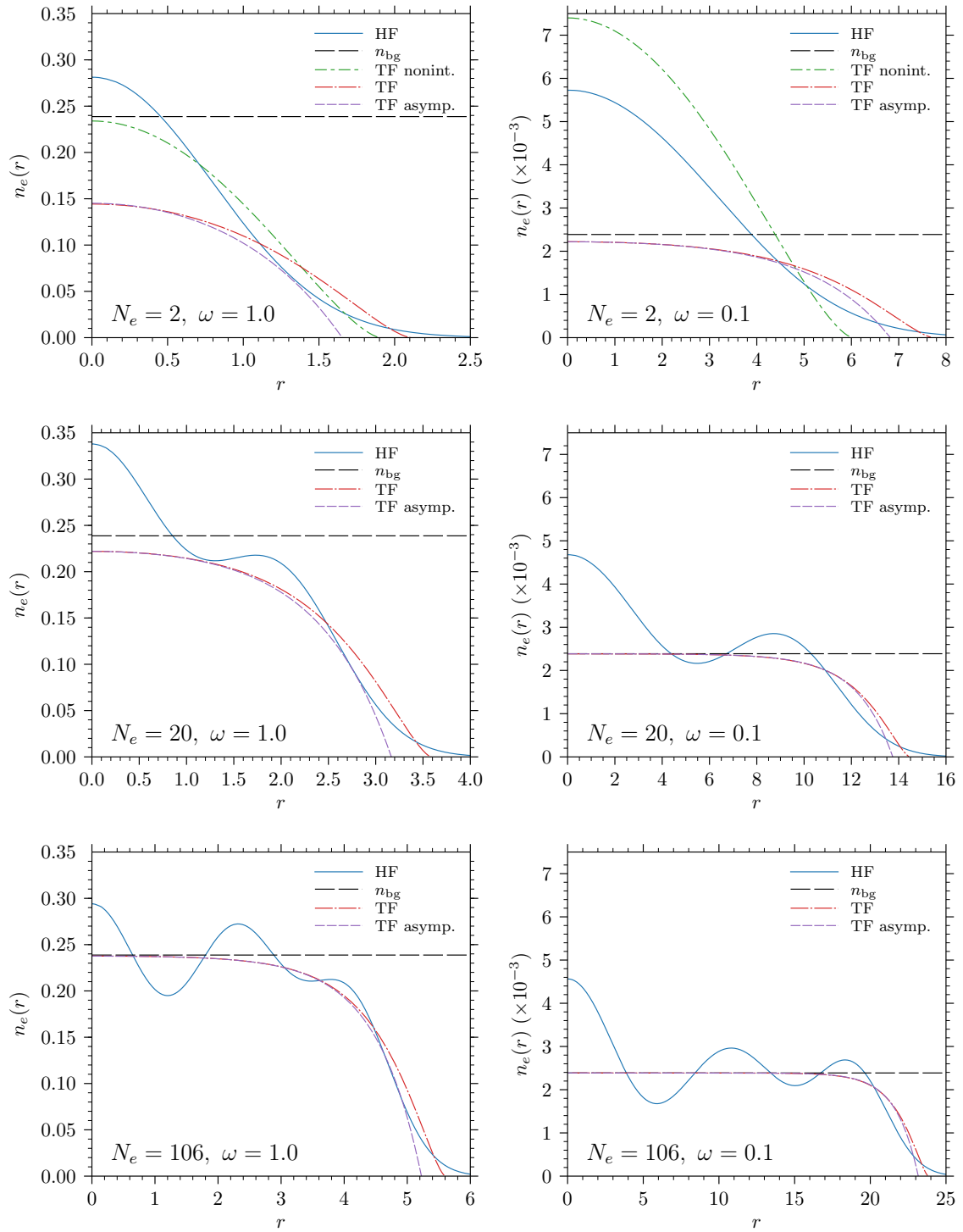


Figure 9. Electron number density curves for systems with $\omega = 1.0$ (left panels), and $\omega = 0.1$ (right panels), and different numbers of electrons (indicated in bottom left of each panel). Equivalent background density $n_{\text{bg}} = 3\omega^2/4\pi$ (horizontal dashed line); Hartree-Fock result (blue solid line); Thomas-Fermi non-interacting model Eqn. (17) (green dashed-dotted line in top left panel only), Thomas-Fermi result, i.e., the solution of Eqn. (14) (red dashed-dotted line), and Thomas-Fermi asymptotic result Eqn. (18) (purple dashed line).

results calculated using a similar Hartree-Fock method using the *hfgr* code [19], but in all cases the new B-spline values of BSHF are closer to the tabulated reference values.

Table 5. Static dipole polarizability of neutral noble gas atoms calculated using a set of 40 B-splines of order 6 compared against the *hfgr* code of Amusia & Chernysheva and reference values [19, 29].

Atom	B-splines	hfgr [19]	Ref. [29]
He	0.997236	0.997167	1.3837675
Ne	1.974636	1.973492	2.6717
Ar	10.140367	10.13132	11.0747
Kr	15.861810	15.84444	16.7656

5.2. Atomic Clusters

Studying systems with multiple atoms would ideally be carried out using full quantum molecular calculations in which the nucleus of each atom and its associated electrons are all treated independently. Such calculations can be expensive. A (somewhat crude but inexpensive) approximation for clusters of atoms of a single element is to use the harmonic potential, as previously described in Sec. 4.

The static dipole polarizabilities for closed-shell systems with N electrons and a positive harmonic background potential for various values of ω are shown in Table 6. However, as the number of electrons in the system increases the effects of screening become more important, and this is underestimated in the HF approximation where electron correlations are not taken into account. The polarizabilities of the same systems were recalculated in the Random Phase Approximation (RPA), which includes a summation of electron-hole diagrams effectively describing the change in the electric field due to the interaction between electrons [30]. These results are shown in Table 7.

This harmonic model can be compared to experiment if we relate the parameter ω to the radius of a physical system, in this case a cluster of N sodium atoms; modelled, as previously, as a background of N singly-ionised cations and N independent electrons. Assuming the ions are evenly distributed in a sphere, we assign a radius of $R = N^{1/3}r_S$, where $r_S = 4a_0$ for Na. This gives $\omega = 0.125$; the static dipole polarizability for this system against the number of atoms, N , is shown in Fig. 10 (also see Table 8.) Experimental values from Knight *et al.* [31], and Tikhonov *et al.* [32] are also shown. The harmonic RPA calculations appear to follow a linear trend, similar to experiment but consistently underestimating α by $\sim 30\%$. Note also that there is no evidence of shell structure shown in previous calculations [33].

5.3. Jellium model

The harmonic model results can easily be improved by using the jellium model, rather than a constant positive harmonic background. In the jellium model the harmonic

Table 6. Static dipole polarizability in the Hartree-Fock approximation for electrons (closed electron orbitals up to and including that shown in the first column) in a harmonic well of frequency ω .

$N(nl)\backslash\omega$	0.1	0.125	0.2	0.4	0.6	0.8	1.0
2 (1s ²)	133.3161	87.1466	35.6765	9.5381	4.4028	2.5423	1.6599
8 (+ 2p ⁶)	998.9175	637.8120	247.2313	60.6943	26.5988	14.7960	9.3834
18 (+ 3d ¹⁰)	3244.2195	2056.7788	783.6019	186.3943	79.9463	43.7488	27.3808
20 (+ 2s ²)	3971.6733	2512.6102	952.2023	224.1820	95.3890	51.8094	32.1833
34 (+ 4f ¹⁴)	8237.8046	5205.9795	1967.3688	460.0682	194.6671	105.2793	65.1895
40 (+ 3p ⁶)	11526.4943	7257.9212	2714.9067	624.5585	261.7499	140.7227	86.8077
58 (+ 5g ¹⁸)	18721.1653	11772.8365	4408.5228	1015.7400	425.4560	228.4397	140.7094
68 (+ 4d ¹⁰)	25829.9106	16182.1026	6015.1382	1368.5965	568.4620	303.3674	186.0353
70 (+ 3s ²)	27636.3551	17281.3058	6406.1312	1452.8810	601.9823	320.4740	196.0164
92 (+ 6h ²²)	38987.7679	24350.1336	9036.0681	2056.8043	853.4749	454.6450	278.1381
106 (+ 5f ¹⁴)	51155.2294	31752.8390	11704.7165	2647.6584	1093.6746	580.5109	354.0825

Table 7. Static dipole polarizability in the RPAE approximation for electrons (closed electron orbitals up to and including that shown in the first column) in a harmonic well of frequency ω .

$N(nl)\backslash\omega$	0.1	0.125	0.2	0.4	0.6	0.8	1.0
2 (1s ²)	200.1095	128.0235	50.0818	12.5535	5.5955	3.1568	2.0263
8 (+ 2p ⁶)	799.9134	511.9628	199.9768	49.9847	22.2100	12.4900	7.9917
18 (+ 3d ¹⁰)	1799.6485	1151.8284	449.9723	112.4934	49.9947	28.1202	17.9955
20 (+ 2s ²)	1999.6429	1279.8055	500.0243	125.0370	55.5871	31.2772	20.0238
34 (+ 4f ¹⁴)	3398.8268	2175.3945	849.9711	212.5311	94.4721	53.1488	34.0207
40 (+ 3p ⁶)	3998.2571	2559.1648	999.8695	249.9788	111.0975	62.4889	39.9904
58 (+ 5g ¹⁸)	5796.3381	3710.2519	1449.7408	362.4719	161.0975	90.6149	57.9917
68 (+ 4d ¹⁰)	6795.1135	4349.5667	1699.6608	424.9729	188.8789	106.2433	67.9942
70 (+ 3s ²)	6994.9137	4477.1771	1749.6900	437.5068	194.4641	109.3949	70.0183
92 (+ 6h ²²)	9191.0181	5884.4769	2299.3879	574.9845	255.5705	143.7665	92.0160
106 (+ 5f ¹⁴)	10588.4735	6777.5321	2649.3053	662.4808	294.4547	165.6423	106.0156

background potential is limited to the defined radius of the system, R , and a Coulomb potential is used outside of this radius:

$$V(r) = \begin{cases} -\frac{N}{2R} \left[3 - \left(\frac{r}{R} \right)^2 \right] & r \leq R \\ -\frac{N}{r} & r > R \end{cases} . \quad (29)$$

The harmonic model results in greater confinement of the electrons, thus reducing the value of α . In the jellium model the electrons can more easily spill over beyond the system radius, R , increasing the polarizability and giving better agreement with experiment. Notably, the calculated values show evidence of shell structure and the corresponding computational results by Guet and Johnson are in excellent agreement with these new calculations [34].

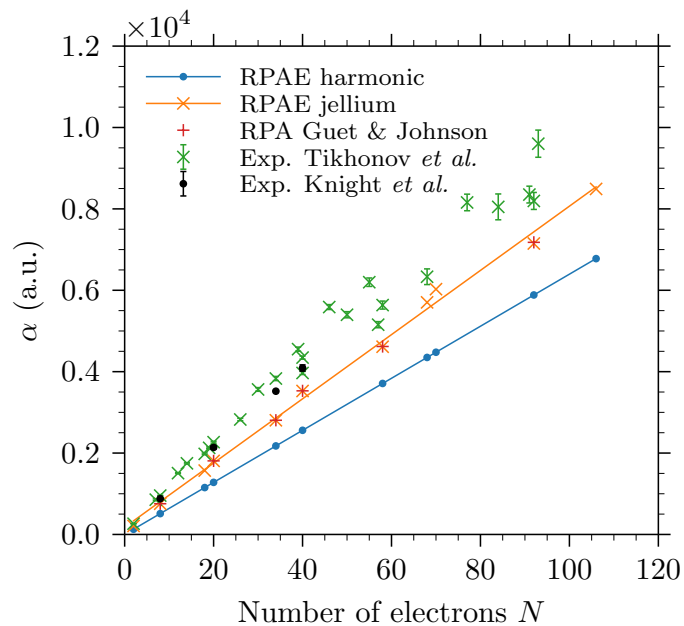


Figure 10. Static dipole polarizability of a cluster of N sodium atoms in the RPAE and jellium approximations benchmarked against similar calculations by Guet and Johnson [34]. Data from two experiments, Tikhonov *et al.* [32], and Knight *et al.* [31], and the results of the harmonic model are shown for comparison. Also see Table 8.

Table 8. Static dipole polarizabilities of a cluster of N sodium atoms in the RPAE and jellium approximations, with similar calculations by Guet and Johnson [34] and experimental results from Tikhonov *et al.* [32], and Knight *et al.* [31]. All polarizability values are in atomic units (a_0^3).

N	Calculations		Experiment	
	Present	Ref. [34]	Knight <i>et al.</i>	Tikhonov <i>et al.</i>
2	208.7455	–	–	264.5 ± 0.0
8	754.8100	755	879 ± 17	955.5 ± 6.0
18	1569.7228	–	–	1979.9 ± 20.4
20	1807.8457	1808	2138 ± 43	2267.4 ± 22.6
34	2805.5966	2806	3520 ± 17	3831.7 ± 51.4
40	3525.5402	3529	4090 ± 77	3968.0 ± 37.7 4345.9 ± 37.7
58	4613.1918	4619	–	5636.2 ± 98.6
68	5702.8570	–	–	6332.6 ± 192.7
70	6026.9162	–	–	–
92	7149.6181	7178	–	8195.2 ± 208.6
106	8490.2581	–	–	–

6. Summary and outlook

An approach to the numerical solution of the Hartree-Fock equations that relies on gradually increasing the electron-electron interaction to its true value, has been presented and found to give good numerical accuracy and fast and robust convergence.

for neutral atoms, negative ions and electrons confined in harmonic potentials (for which comparison with the Thomas-Fermi model was made). The completeness of the manifold of excited-state wavefunctions was tested by calculating the static dipole polarizability of a range of neutral noble gas atoms in the static and Random-Phase Approximations, showing results consistent with previous methods. The HF basis states can be used in higher-order diagrammatic many-body calculations for systems with arbitrary central potentials, enabling calculations of electrons and positrons confined in electron gas [12].

References

- [1] Hartree D R 1928 *Math. Proc. Cambridge Phil. Soc.* **24** 111
- [2] Slater J C 1930 *Phys. Rev.* **35** 210
- [3] Fock V 1930 *Z. Phys.* **61** 126
- [4] Boyle J and Pindzola M 1998 *Many-body atomic physics* (Cambridge University Press)
- [5] Cheng Y, Tang L Y, Mitroy J and Safronova M S 2014 *Phys. Rev. A* **89** 012701
- [6] Gribakin G F and Ludlow J 2004 *Phys. Rev. A* **70** 032720
- [7] Green D G, Ludlow J A and Gribakin G F 2014 *Phys. Rev. A* **90** 032712
- [8] Green D G, Swann A R and Gribakin G F 2018 *Phys. Rev. Lett.* **120** 183402
- [9] Theel F, Karamatskou A and Santra R 2017 *Chaos* **27** 123103
- [10] Waide D, Green D and Gribakin G 2020 *Comp. Phys. Commun.* **250** 107112
- [11] Ahlrichs R 1975 *Chem. Phys. Lett.* **34** 570
- [12] Makkonen I, Ervasti M M, Siro T and Harju A 2014 *Phys. R. B* **89** 041105
- [13] Gribakin G F and Ludlow J 2004 *Phys. Rev. A* **70** 032720
- [14] Green D G, Ludlow J A and Gribakin G F 2014 *Phys. Rev. A* **90** 032712
- [15] Goldstone J 1957 *Proc. Roy. Soc. A* **239** 237
- [16] Dickhoff W H and Neck D V 2008 *Many body theory exposed! - Propagator Description of Quantum Mechanics in Many-Body Systems - 2nd ed.* (World Scientific, Singapore)
- [17] Zubiaga A, Ervasti M M, Makkonen I, Harju A, Tuomisto F and Puska M J 2016 *J. Phys. B* **49** 064005
- [18] de Boor C 1978 *A Practical Guide to Splines* (Springer-Verlag, New York)
- [19] Amusia M and Chernysheva L V 1997 *Computation of Atomic Processes* (IoP Publishing, Bristol)
- [20] Saito S L 2009 *At. Data Nucl. Data Tables* **95** 836
- [21] Radtsig A A and Smirnov B M 1986 *Parameters of Atoms and Atomic Ions Handbook* (Energoatomizdat, Moscow)
- [22] Kramida A, Yu Ralchenko, Reader J and NIST ASD Team 2015 NIST Atomic Spectra Database (ver. 5.3), [Online]. Available: <http://physics.nist.gov/asd> [2017, May 22]. National Institute of Standards and Technology, Gaithersburg, MD.
- [23] Handy N C, Marron M T and Silverstone H J 1969 *Phys. Rev.* **180** 45
- [24] Dzuba V A, Flambaum V V and Silvestrov P G 1982 *J. Phys. B: At. Mol. Phys.* **15** L575
- [25] Kozlov M G and Flambaum V V 2013 *Phys. Rev. A* **87** 042511
- [26] Thomas L H 1927 *Math. Proc. Cambridge Phil. Soc.* **23** 542
- [27] Brack M 1993 *Rev. Mod. Phys.* **65** 677
- [28] Flambaum V V and Samsonov I B 2021 Radiation from matter-antimatter annihilation in the quark nugget model of dark matter arXiv:2108:00652 [hep-ph]
- [29] Johnstone A H (ed) 1991 *CRC Handbook of Chemistry and Physics-69th Edition* (John Wiley & Sons, Ltd.)
- [30] Bohm D and Pines D 1953 *Phys. Rev.* **92** 609
- [31] Knight W D, de Heer W A, Clemenger K and Saunders W A 1985 *Solid State Comm.* **53** 445
- [32] Tikhonov G, Kasperovich V, Wong K and Kresin V V 2001 *Phys. Rev. A* **64** 063202

- [33] de Heer W A, Knight W D, Chou M Y and Cohen M L 1987 Electronic Shell Structure and Metal Clusters *Solid State Physics* vol 40 ed Ehrenreich H and Turnbull D (Academic Press) p 93
- [34] Guet C and Johnson W R 1992 *Physical Review B* **45** 11283